Solar Energy Materials and Solar Cells 203 (2019) 110175

Contents lists available at ScienceDirect

Solar Energy Materials and Solar Cells

journal homepage: www.elsevier.com/locate/solmat

Influence of $NaErF_4$@$NaYF_4$ nanoparticles doping on performances of $Cu_2ZnSn(S,Se)_4$ solar cell

Di Liu[a], Xiaohui Zhang[a], Wei Qin[a], Bin Yao[a,b,*], Langping Tu[c,**], Yongfeng Li[a], Gang Wang[d], Hongmei Luan[a], Xianggui Kong[c], Zhanhui Ding[a], Yuhong Jiang[a], Haifeng Zhao[c], Zhenzhong Zhang[c], Ligong Zhang[c]

[a] Key Laboratory of Physics and Technology for Advanced Batteries (Ministry of Education), College of Physics, Jilin University, Changchun, 130012, China
[b] State Key Lab of Superhard Material, College of Physics, Jilin University, Changchun, 130012, China
[c] State Key Laboratory of Luminescence and Applications, Changchun Institute of Optics, Fine Mechanics and Physics, Chinese Academy of Sciences, No.3888 Dongnanhu Road, Changchun, 130033, China
[d] State Key Laboratory of Rare Earth Resource Utilization, Changchun Institute of Applied Chemistry, Chinese Academy of Sciences, 5625 Renmin Street, Changchun, 130022, China

ARTICLE INFO

Keywords:
Solar cell
CZTSSe
$NaErF_4$@$NaYF_4$
Photo-generated current
First principle calculation

ABSTRACT

We report the improvement of $Cu_2ZnSn(S,Se)_4$ (CZTSSe) solar cells via doping $NaErF_4$@$NaYF_4$ (NEYF) nanoparticles. The NEYF nanoparticles were doped into the CZTSSe layer as an absorber in a solar cell with the conventional structure of SLG/Mo/absorber/CdS/i-ZnO/ITO/Al. It is found that NEYF doping could increase open circuit voltage (V_{OC}), short circuit current density (J_{SC}) and fill factor (FF) of the CZTSSe solar cell, which enables the best power conversion efficiency (PCE) increase from 4.03% of CZTSSe solar cell up to 7.10%. For the solar cell with a NEYF-doped CZTSSe (CZTSSe:NEYF) absorber, the improved V_{OC} and J_{SC} are mainly due to the decrease in reverse saturation current density (J_0) and the improvement in photocurrent density (J_L) brought by NEYF doping, while the enhancement in fill factor should be ascribed to the decreased series resistance (R_s). The mechanisms of change in the J_0, J_L, R_s and band gap (E_g) from NEYF doping are discussed in detail by comparative study of composition, structure and electrical properties of the CZTSSe:NEYF and CZTSSe films as well as interfacial structures of CZTSSe:NEYF and CZTSSe solar cells in the present work.

1. Introduction

Kesterite $Cu_2ZnSn(S,Se)_4$ (CZTSSe) is well recognized as a promising absorber material of candidate for replacing CIGS due to its earth-abundant constituents, high absorption coefficient ($> 10^4\ cm^{-1}$), tunable band gap (1.0–1.5 eV) and eco-friendly fabrication methods. However, even the top power conversion efficiency (PCE) has reached 12.6% in 2014, it's still a long way to go to catch up with the top PCE (22.6%) of CIGS solar cell [1,2]. It has been demonstrated that low open circuit voltage (V_{OC}) or large V_{OC} deficiency (ΔV_{OC}, equal to E_g/q-V_{OC}, the E_g is bandgap of CZTSSe and q is electron charge) is the biggest hurdle preventing CZTSSe solar cells from achieving higher efficiency [3–5]. In the last decade, many approaches have been used to improve V_{OC}. For instance, some researchers increased V_{OC} by using optimizing elemental ratios of CZTSSe, improving crystal quality of absorbers, passivizing superficial defects of CZTSSe, lessening secondary phases and optimizing band alignment between absorber and buffer/back electrode [5–8]. Some literatures reported that improvement of the V_{OC} could be achieved by enhancing electrical properties of CZTSSe through alkali metal element (Li Na, Rb) doping [9–11] or changing electron structure through tuning defects distribution with Ag element doping [12]. Although great progress in V_{OC} improvement have been made by these trials through decreasing electrical loss, the overall PCE still haven't excessed 12.6% by now.

Recently, some literatures reported enhancement of PCE of various solar cell systems by using up-conversion material's unique ability that converting NIR light to visible light [13,14]. Xu Chen et al. used $LiYF_4$:Yb^{3+}, Er^{3+} single crystal as independent luminescent upconverter and improved the perovskite solar cells' efficiency by 7.9% through placing the single crystal in front of the perovskite solar cells; Ho^{3+}-Yb^{3+}-F- tri-doped TiO_2 photoanode were designed and applied in dye-sensitized solar cells by Jia Yu et al., and its application enhanced

* Corresponding author. State Key Lab of Superhard Material, and College of Physics, Jilin University, Changchun, 130012, China.
** Corresponding author.
E-mail addresses: binyao@jlu.edu.cn (B. Yao), tulangping@163.com (L. Tu).

https://doi.org/10.1016/j.solmat.2019.110175
Received 22 May 2019; Received in revised form 10 September 2019; Accepted 12 September 2019
Available online 18 September 2019
0927-0248/

the devices' efficiency from 7.19% to 9.91% [13,15]. These results imply that applying these near infrared (NIR) light to enhance photocurrent may be a feasible solution to improve CZTSSe solar cells' efficiency.

It is well known that the band gap of CZTSSe is about 1.0 eV–1.5 eV and so the photons with energy lower than 1.0 eV (wavelength above 1240 nm) cannot be absorbed by CZTSSe to generate photocurrent. $NaErF_4$@$NaYF_4$ (denoted as NEYF) with core-shell(~20 nm $NaErF_4$ core and ~5 nm $NaYF_4$ shell) nanostructure is a novel up-conversion material which could be excited by multi NIR light (~800 nm, ~980 nm, ~1530 nm) and then emit red light (~650 nm) [16]. When it combines with CZTSSe in a suitable mode, it may extend wavelength range of light absorbed by CZTSSe in principle and so increase PCE by enhancement of photo-generated current. Besides, NEYF contains Na ions, which have been illustrated by many literatures to be beneficial for increase in V_{OC} and FF of CZTSSe and CIGS solar cells [17–19]. These unique properties may make NEYF doping suitable for improving CZTSSe solar cells' PCE in theory.

Based on the two points mentioned above, we tried to improve PCE of CZTSSe solar cell by NEYF doping in the present work. To investigate the influence of NEYF doping on the performance of CZTSSe devices, two applying modes are adopted to prepare CZTSSe solar cells. One is applying NEYF doped CZTSSe thin films as absorbers of solar cells (corresponding devices are denoted as CZTSSe:NEYF), and another is inserting NEYF between absorbers and back electrodes (corresponding devices are denoted as CZTSSe/NEYF). It is found that NEYF doping can improve V_{OC}, J_{SC} and FF of CZTSSe solar cell, thereby enhances PCE from 4.03% to 7.10%, while inserting NEYF increases PCE little. Mechanism of effects of the NEYF doping on the PCE of CZTSSe solar cell is also studied in detail.

2. Experimental

2.1. Reagents

$LnCl_3{\cdot}6H_2O$(Ln: Y, Er > 99%), Ln_2O_3(Ln: Y, Er > 99%), oleic acid (OA, 90%), 1-ocatadecene(ODE, 90%), oleylamine (OM, 90%), sodium trifluoroacetate (98%), trifluoroacetic acid (99%), copper(II) acetate monohydrate, zinc(II) chloride, tin(II) chloride dehydrate, thiourea, Dimethyl sulfoxide (DMSO) and monoethanolamine(MEA) were purchased from Sigma-Aldrich and used without further purification. NaOH (> 98%), NH_4F (> 98%), methanol, ethanol and cyclohexane were purchased from GFS Chemical.

2.2. Synthesis of the β-core–shell $NaErF_4$@$NaYF_4$ nanoparticles

The $NaErF_4$@$NaYF_4$ core–shell (or core–shell–shell) (NEYF) nanoparticles, individual $NaErF_4$ nanoparticles (NEF) and $NaYF_4$ nanoparticles (NYF) were prepared following a previous approach in the reported literatures [16,19,20].

2.3. Preparation of NEYF-doped CZTSSe thin films

2.3.1. Synthesis of NEYF-Cu-Zn-Sn-S precursor solution

A Cu–Zn–Sn–S precursor solution was synthesized by dissolving copper (II) acetate monohydrate, sodium acetate, zinc (II) chloride, tin (II) chloride dehydrate, thiourea and MEA in DMSO, where the MEA was used as stabilizer. And the mole ratio of Cu:Zn:Sn:S were 6:4.4:3.75:30 in the precursor. Considering the loss during experiments, to obtain the NEYF-Cu-Zn-Sn-S precursor solution with different NEYF concentration, the NEYF were added in the Cu–Zn–Sn–S solution according to their concentration of 0, 5 mg/ml and 10 mg/ml, respectively.

2.3.2. Preparation of $NaErF_4$@$NaYF_4$-doped Cu–Zn–Sn–S thin films

The NEYF-doped CZTSSe thin films were prepared by spin-coating NEYF-Cu-Zn-Sn-S precursor solutions with NEYF concentration of 0, 5 mg/ml and 10 mg/ml, respectively, onto soda lime glass (SLG) substrates for 30 s in a glove box filled with nitrogen, then annealing at 300 °C for 3 min on a hot plate. The spin-coating and annealing were repeated 10 times to get a ~1-μm thick thin film.

2.3.3. Preparation of $NaErF_4$@$NaYF_4$-doped $Cu_2ZnSn(S,Se)_4$ thin films

NEYF-doped $Cu_2ZnSn(S,Se)_4$ thin films were prepared by selenizing NEYF-doped Cu–Zn–Sn–S thin films for 11 min at 550 °C. Firstly, NEYF-doped Cu–Zn–Sn–S thin films were placed in a graphite box that contains 150 mg Se powder, then transported to a rapid thermal processing furnace and finally annealed at 550 °C for 11min. The NEYF-doped $Cu_2ZnSn(S,Se)_4$ thin films prepared by using NEYF-Cu-Zn-Sn-S precursor solution with concentration of 0, 5 and 10 mg/ml are denoted as CZTSSe, CZTSSe@5 mg and CZTSSe@10 mg, respectively.

2.4. Preparation of three kinds of $Cu_2ZnSn(S,Se)_4$ based solar cells

Three kinds of CZTSSe-based solar cell with the conventional structure of SLG/Mo/absorber/CdS/i-ZnO/ITO/Al were prepared by using CZTSSe and the CZTSSe@5 mg as absorbers and inserting NEYF between CZTSSe and Mo back electrode, respectively, which are denoted as CZTSSe, CZTSSe:NEYF and CZTSSe/NEYF solar cells, respectively. For the CZTSSe and CZTSSe:NEYF solar cells, firstly, the CZTSSe or NEYF-doped $Cu_2ZnSn(S,Se)_4$ absorbers were grown on Mo-coated SLG using the method mentioned in 2.3.1–2.3.3, then, 60 nm-thick CdS films were deposited as buffer layer with chemical bath depositing. After that, i-ZnO(70 nm) and ITO(250 nm) were sputtered on the top of CdS layer. Finally, An Al grid electrode (~1.0 μm) was evaporated on top of ITO by evaporation deposited method. For the CZTSSe/NEYF solar cell, NEYF was spin-coated and annealed at 200 °C for once on Mo-coated SLG firstly with 5 mg/ml NEYF contained DMSO solution and then CZTSSe was grown through methods mentioned in 2.3.1–2.3.3. After that, CdS, i-ZnO, ITO and Al was grown sequentially with the same processes mentioned above.

2.5. Preparation of individual $NaErF_4$, $NaYF_4$ and Na doped CZTSSe solar cells

First, $NaErF_4$(NEF), $NaYF_4$(NYF) and Na doped CZTSSe thin films were prepared through methods mentioned in 4.3.1–4.3.3 with 5 mg/ml NEF, 5 mg/ml NYF and 5(10,15)*M_r(sodium acetate)/M_r(NEYF) mg/ml (for keeping same Na content with NEYF doped CZTSSe) contained DMSO solution, respectively. Then, NEF, NYF and Na doped CZTSSe solar cells with convention structure were prepared with NEF, NYF and Na doped CZTSSe thin films as absorbers through methods mentioned in 4.4 and are denoted as CZTSSe:NEF, CZTSSe:NYF and CZTSSe:Na respectively.

2.6. Characterization

The power conversion efficiency (PCE) of the solar cells were determined by analysis of current density–voltage (J–V) curves measured with Keithley 2400 source meter and a solar simulator (Abet Sun 2000; AM 1.5). The light intensity of the simulator was calibrated to 100 mW/cm^2 using a Newport optical power meter (model 842-PE) certified by Newport. The external quantum efficiency (EQE) and reflection curves were measured with a Zolix SCS100 QE system equipped with a 150 W xenon light source, a lock-in amplifier and an integrating sphere. Scanning electron microscopy (SEM, Hitachi S-4800) was used to characterize morphology of cross section of the solar cells. X-Ray diffractometer (XRD) measurements were performed to characterize thin films' crystal structures. The composition of thin films was measured by energy dispersive X-ray spectroscopy (EDS) system (EDAX Genesis 2000).The compositions and valance states of elements at the surfaces of the thin films were measured by X-Ray photoelectron spectroscopy

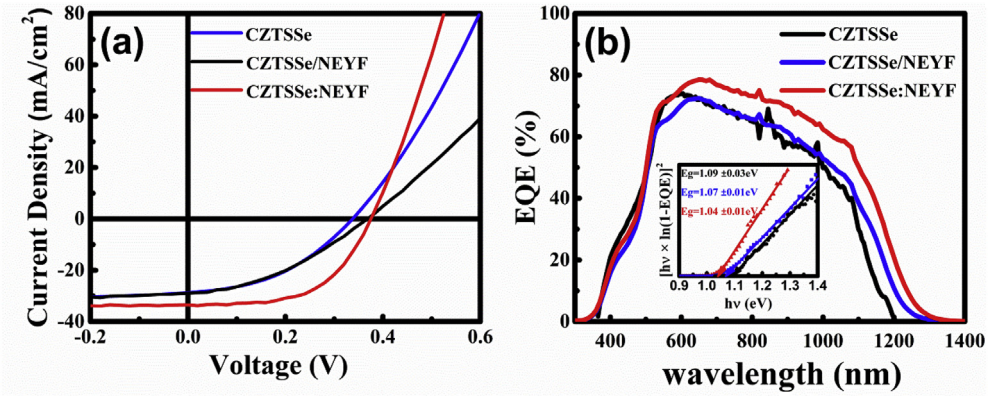

Fig. 1. J-V curves (a) andEQE response (b) of CZTSSe, CZTSSe/NYF and CZTSSe:NEYF solar cells with best PCE, and the inset in (b) is the plot of $[h\nu \times ln(1 - EQE)]^2$ verses $h\nu$.

(XPS) with Al Kα = 1486.6 eV x-ray radiation source, and all XPS spectra were calibrated by the C1s peak(284.6 eV). Hall Effect measurement system with the van der Pauw configuration was used to measure electrical properties of samples.

3. Results and discussions

The devices' J-V curves were measured to investigate the influence from NEYF nanoparticles and their applying modes. The J-V curves of each kind of device with the best PCE are shown in Fig. 1(a), where their photovoltaic parameters, including open circuit voltage (V_{OC}), short circuit current density (J_{SC}), fill factor (FF) and electric parameters including series resistivity (R_s), shunt conductivity (G_{sh}) and reverse saturated current density (J_0) are extracted, as listed in Table 1. The statistical distributions of these photovoltaic and electric parameters for all of the three kinds of solar cells are shown in Figs. 1S and 2S (in Supporting Information), respectively. The average value of each kind of devices' photovoltaic and electric parameters is listed in the bracket of Table 1. It is indicated from Table 1 that the best PCE of the CZTSSe solar cells can be improved obviously from 4.03 to 7.10% by doping NEYF into CZTSSe, but increased little (only to 4.067%) by inserting NEYF between the CZTSSe and Mo. According to Table 1, The main reason of improvement in PCE for CZTSSe:NEYF solar cell is its enhanced V_{OC}, J_{SC} and FF, while for CZTSSe/NEYF solar cell is its improved J_{SC} and FF. Besides, it also can be indicated that the average value of devices' parameters and the value of best devices' parameters share the same trend, which demonstrates the reliability of the results.

In order to understand the mechanism of increase in PCE, EQE of the three kinds of solar cell with the best PCE are measured, as shown in Fig. 1(b). With the EQE data, bandgaps (E_g) and open-circuit voltage deficits ($\Delta V_{OC} = E_g/q\text{-}V_{OC}$) of the three solar cells are calculated [21], as shown in the inset of Fig. 1(b) and Table 1. These results indicate that the NEYF doping increases V_{OC} while decreases E_g, which contracts with the well-known common relationship between E_g and V_{OC} and demonstrates that the increased V_{OC} does not mainly come from contribution of E_g. Since V_{OC} can also be influenced by electronical parameters; the improvement in V_{OC} induced by NEYF doping should be ascribed to the change in electronic parameters. Based on electrical parameters in Table 1 and relation between V_{OC} with G_{sh} and J_0:

$$G_{sh}V_{oc} = J_L - J_0\left[\exp\left(\frac{qV_{oc}}{AkT}\right) - 1\right] \quad (1)$$

where J_L is photo-generated current density, A ideal factor of diode, q is electronic charge, k Boltzmann constant and T temperature, it is deduced from Equation (1) and Table 1 that the increased V_{OC} in CZTSSe:NEYF solar cells is mainly due to its decrease in J_0 and improvement of J_L, while the decrease in V_{OC} of the CZTSSe/NEYF solar cells should not only be attributed to its decreased band gap but also to enhanced J_0.

From Fig. 1(b) it is found that the difference in EQE response between CZTSSe and CZTSSe/NEYF solar cells occurs in the wavelength range of about 1100–1300 nm. Combing data in Table 1, it is inferred that the increased J_{SC} is mainly related to the decrease in E_g for the CZTSSe/NEYF solar cell. However, compared to CZTSSe solar cell, CZTSSe:NEYF solar cell not only has smaller E_g but higher EQE in the wavelength range of 520–1400 nm. This means that the increased J_{SC} of the CZTSSe:NEYF solar cell should come from decreased E_g as well as increased J_L and decreased J_0, based on electrical parameters in Table 1 and the relation between J_{SC} with R_s, G_{sh}, J_L and J_0 expressed as:

$$(1 + R_sG_{sh})J_{sc} = J_L - J_0\left[\exp\left(\frac{qJ_{sc}R_s}{AkT}\right) - 1\right] \quad (2)$$

It is well known that FF increases with decreasing series resistivity (R_s) and shunt conductivity (G_{sh}). From Table 1 it can be seen that the FF increases with decreasing Rs but not with decreasing G_{sh}, which implies that the increased FF mainly comes from the decrease in R_s.

The above discussions about data in Table 1 indicate that the CZTSSe:NEYF solar cells have better performance than CZTSSe and CZTSSe/NEYF solar cells. So it's necessary to investigate the mechanism of influences from NEYF doping on E_g, J_L and electric parameters of the CZTSSe solar cells for further understanding about how NEYF doping affects the performance of CZTSSe solar cells.

To further tackle these problems, CZTSSe thin film doped with various NEYF content were prepared by using CZTSSe precursor solutions with nominal NEYF concentrations of 0, 5 and 10 mg/ml, and denoted as CZTSSe, CZTSSe@5 mg, CZTSSe@10 mg, respectively. The composition, structure, and electric properties of these thin films were characterized.

Table 2 summarizes the element ratios of NEYF, CZTSSe, NEYF-doped CZTSSe thin films. It indicates that there are Na, Er, Y and F

Table 1
Photovoltaic and electrical parameters of CZTSSe, CZTSSe/NEYF and CZTSSe:NEYF solar cells with best PCE and average values of the parameters of each kind of solar cells.

Devices	CZTSSe	CZTSSe/NEYF	CZTSSe:NEYF
V_{OC} (mV)	368(362.8)	342(333.7)	378(368.7)
J_{SC} (mA/cm^2)	28.94(27.74)	29.37(28.87)	33.51(33.68)
FF (%)	37.84(36.76)	40.47(39.15)	56.04(53.75)
PCE (%)	4.03(3.70)	4.07(3.77)	7.10(6.66)
R_s (Ωcm^2)	4.67(4.58)	2.10(2.96)	1.03(1.12)
R_{sh} (Ωcm^2)	961.5(516.8)	201.6(189.8)	434.8(366.3)
J_o (mA/cm^2)	0.067(0.105)	0.128(0.120)	0.028(0.0627)
A	2.20	2.45	1.90
E_g (eV)	1.09	1.07	1.04
ΔV_{OC} (eV)	0.72(0.73)	0.73(0.74)	0.66(0.67)

Table 2
Compositions of CZTSSe, CZTSSe@5 mg, CZTSSe@10 mg thin films and pure NEYF measured by EDS.

Samples	CZTSSe (at%)	CZTSSe @5 mg (at%)	CZTSSe of CZTSSe @5 mg (at%)	NEYF of CZTSSe @5 mg (at%)	CZTSSe@10 mg (at%)	CZTSSe of CZTSSe@10 mg (at%)	NEYF of CZTSSe @10 mg (at%)	NEYF (at%)
Cu	21.1	18.32	19.23	–	18.37	19.71	–	–
Zn	12.34	12.05	12.67	–	12.16	13.04	–	–
Sn	11.97	10.62	11.161	–	10.37	11.12	–	–
S	4.21	2.3	2.42	–	1.45	1.56	–	–
Se	50.38	51.89	54.52	–	50.87	54.57	–	–
Cu/Zn + Sn	0.868	0.808	0.808	–	0.815	0.815	–	–
Zn/Sn	1.031	1.135	1.13	–	1.173	1.173	–	–
S/S + Se	0.077	0.042	0.042	–	0.028	0.028	–	–
F	–	2.32	–	48.24	3.88	–	57.3	52.64
Na	–	0.37	–	7.69	0.55	–	8.1	20.67
Y	–	1.66	–	34.51	1.93	–	28.5	19.35
Er	–	0.46	–	9.56	0.41	–	6.1	7.33

Notes: The data in CZTSSe of CZTSSe@5(or 10 mg) column shows atomic percent of Cu, Zn, Sn, S and Se in CZTSSe@5(10 mg) thin films without taking F, Na, Y and Er into account; The data in NEYF of CZTSSe@5(or 10 mg) column shows atomic percent of F, Na, Y and Er in CZTSSe@5(10 mg) thin films without taking Cu, Zn, Sn, S and Se into account.

elements in the NEYF doped CZTSSe thin films. To characterize doping behaviors of the Na, Er, Y and F in the CZTSSe thin films, XRD and Raman spectrum measurements were performed for the CZTSSe thin films with different NEYF concentration.

Fig. 2(a) shows the XRD patterns of the CZTSSe, CZTSSe@5 mg and CZTSSe@10 mg thin films grown on Mo coated SLG. Only diffraction peaks of kesterite CZTSSe (labeled ●) and (110) peak of Mo (marked with ♣) are observed in the XRD curves of the CZTSSe@5 mg (middle curve) and CZTSSe@10 mg (top curve), no other XRD peaks including XRD peak of NEYF are observed obviously [16]. However, (100) peak of $MoSe_2$ (marked with ♦) is also observed obviously in XRD curve of the CZTSSe (bottom curve) besides diffraction peaks of CZTSSe and Mo. These indicate that the $MoSe_2$ formed at CZTSSe@5 mg (or10mg)/Mo interface is a little and much less than that in CZTSSe/Mo interface, which is also confirmed by cross section morphologies of the best CZTSSe and CZTSSe:NEYF solar cell, as shown in Fig. 3. It is obvious in Fig. 3 that NEYF doping decreased the thickness of $MoSe_2$ layer between absorber and back electrode. Since the existence of $MoSe_2$ will increase R_s of solar cells, the decreased R_s of CZTSSe:NEYF solar cell should be attributed to its thickness of $MoSe_2$ less than CZTSSe solar cells.

Since the phonon scattering peaks in Raman scattering could shed light on the existence of different phases and defects in CZTSSe thin films, Raman spectra of the CZTSSe, CZTSSe@5 mg and CZTSSe@10 mg films were recorded to determine defects and phase compositions of the films, as shown in Fig. 2(b). For the CZTSSe, only Raman peaks of CZTSSe are observed near 174, 196, 232, 245 and 327 cm^{-1}, no other Raman peak is observed, implying the CZTSSe film consists of a single phase of CZTSSe. However, for NEYF doped CZTSSe films, three Raman peaks located at 373, 408 and 800 cm^{-1} are observed besides Raman peaks of CZTSSe. Moreover, the intensity of the three peaks augments with increasing NEYF doping content. It is reported that the 373 and 408 cm^{-1} are attributed to the vibration of $NaYF_4$, so it is inferred that the peaks are related to $NaYF_4$(NYF) of the NEYF [22]. From Table 2 it is seen that the atomic ratios of F, Na, Y and Er of the NEYF in the CZTSSe@5 mg and CZTSSe@10 mg thin films are much different from those of pure NEYF. The content almost does not change for F and Er, but decreases sharply for Na and increases for Y. These imply that part of the NEYF decompose during selenization process. The sharp decrease in Na is due to diffusion of Na to surface, which will be demonstrated by XPS results later. The increased Y ratio is due to decreased Na. Based on analysis about the Raman spectra and element ratios of the NEYF, it is deduced that only partial NYF of the shell-core NEYF nanoparticles decomposed. The undecomposed NYF nanoparticles might remain as shell of the shell-core structure in the grain boundaries of the CZTSSe.

Compared to the peaks of the CZTSSe, it is found from the inset of Fig. 2(b) that the A1 vibration of Se atoms near 193 cm^{-1} shifts to short wavenumber direction with increasing NEYF content. Similar shift is also observed in XRD pattern, as shown in inset of Fig. 2(a). These indicate that lattice constants increase with increasing NEYF doping

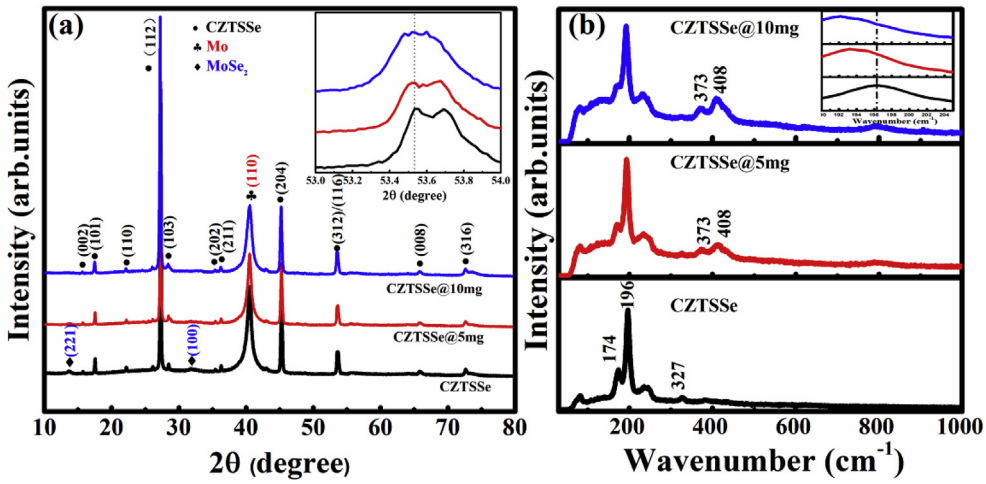

Fig. 2. XRD patterns (a) and Raman spectra (b) of the CZTSSe (bottom), CZTSSe@5 mg (middle) and CZTSSe@10 mg (top) thin films grown on Mo-coated SLG substrates, and inset in Fig. 2(a) shows the enlarged (312) and (116) peaks of CZTSSe, while inset in (b) shows the enlarged A1 vibration of Se (193 cm^{-1}).

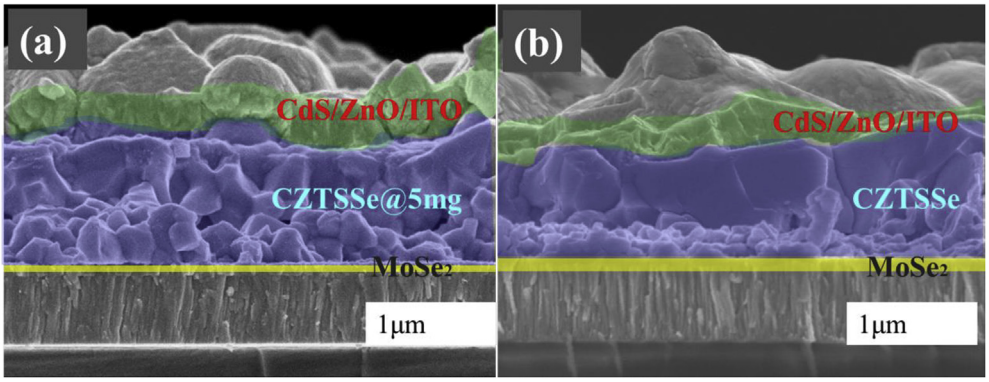

Fig. 3. The SEM characterization of CZTSSe:NEYF (a) and CZTSSe (b) solar cells.

content. It is known that Na^{1+} and Y^{3+} have much larger ionic radius than Cu^{1+}, Zn^{2+} and Sn^{4+} [23]. They would increase lattice constants of the CZTSSe if they are incorporated into CZTSSe in substitutional form. However, even the formation energy of Na_{Cu} and Na_{Zn} defects in CZTSe are very low under Cu-poor and Zn-rich condition, it is demonstrated that Na doped in CZTSSe solar cells mainly exist as secondary phases in lattice boundaries or on the surfaces, other than working as dopants, according to previous literatures [24,25]. As for Y-related defects, their formation energy under Cu-poor condition is higher than 1.0 eV, as shown in Fig. S5 (in Supporting Information), which means that the population of Y related defects in CZTSe lattice is too low to be taken into consideration [26]. Besides, it is indicated from Table S2 (in Supporting Information) that the formation of Y-related secondary phases is inevitable, which means that Y doped in CZTSe should exist as secondary phases [18]. As mentioned above, the NEYF didn't decompose completely. It means that the $NaErF_4$ (NEF) was still enclosed by remained NYF and Er cannot dissolve into CZTSSe. F has smaller ionic radius than S and Se, and cannot increase lattice constants of CZTSSe by substitution for S or Se, so F won't be incorporated into CZTSSe lattice. In fact, it is demonstrated in many experimental reports that F in CZTSSe thin films do not work as dopants [18,27]. Referring to the NaF doping results in CIGS solar cells, it is deduced that the F loss mainly comes from the evaporation of NaF during annealing. It can be seen from Table 2 that the S content decreases with increasing NEYF doping content, resulting in S/(S + Se) ratio of NEYF doped CZTSSe thin films smaller than that of CZTSSe thin film. Based on above analysis, it is concluded that the increased lattice constants should be ascribed to decreased S/(S + Se) ratio bring by NEYF doping.

Many literatures have demonstrated that the E_g of CZTSSe decreases with decreasing S/(S + Se) ratio [28–30]. According to relation between E_g and S/(S + Se) ratio (x) for CZTSSe, CZTS and CZTSe predicted by Chen et al.

$$E_g(CZTSSe) = x\,E_g(CZTS) + (1\text{-}x)\,E_g(CZTSe) - 0.1(1\text{-}x)x \quad (3)$$

where the E_g(CZTSSe), E_g(CZTSe) and E_g(CZTS) represent E_g of CZTSSe, of CZTSe and of CZTS, respectively [30]. E_g(CZTSe) and E_g(CZTS) is 1.0 and 1.5 eV,respectively. Using Equation (3) and S/(S + Se) ratios listed in Table 2, the E_g of CZTSSe, CZTSSe@5 mg and CZTSSe@10 mg thin films are estimated to be 1.032, 1.017 and 1.011 eV, respectively, closed to the E_g calculated through EQE of inset of Fig. 1(b). So, the decrease in the E_g of CZTSSe:NEYF solar cell compared to that of CZTSSe is due to the decreased S/(S + Se) ratio.

It is found from Fig. 2(b) that the relative intensity of Raman peak located at 174 cm^{-1} decrease with increasing content of NEYF, compared with the intensity of Raman peak at 193 cm^{-1}. From Table 2 it is also founded that the Cu/(Zn + Sn) decreases while Zn/Sn increases with increasing NEYF doping content. Combining these results, it is concluded that the relative intensity of the 174 cm^{-1} decreases with decreasing Cu/(Zn + Sn) and increasing Zn/Sn. Some literatures have demonstrated that decrease in density of 174 cm^{-1} peak is attributed to increased beneficial [V_{Cu} + Zn_{Cu}] defect complexes and reduced detrimental [$2Cu_{Zn}$ + Sn_{Zn}] defect complexes, which are induced by decrease in the Cu/(Zn + Sn) and increase in Zn/Sn ratios [31–34]. Based on above discussions, it is concluded that NEYF doping can increase [V_{Cu} + Zn_{Cu}] and decrease [$2Cu_{Zn}$ + Sn_{Zn}] complexes. The change of the defect complexes will affect electrical properties of CZTSSe and thus photo-generated current density J_L, as discussed below.

Table 3 lists electrical parameters of the CZTSSe, CZTSSe@5 mg and CZTSSe@10 mg thin films obtained by Hall effect measurement, which shows that the hole concentration changes with NEYF doping content. It is known that NEYF contains Na element and Na doping has influence on electrical properties of CZTSSe and performance of CZTSSe solar cell. In order to understand influence mechanism of NEYF doping on electrical properties of CZTSSe and performance of CZTSSe solar cell, Na doped CZTSSe (CZTSSe:Na) films with different nominal Na contents and corresponding CZTSSe:Na solar cell devices were prepared by using the same approach as that used for preparation of NEYF doped CZTSSe film and NEYF doped CZTSSe solar cell. The results are shown in Table S1 and Fig. S3. It is found from Table S1 that the hole concentration of the CZTSSe:Na increases with increasing nominal Na content. This is in agreement with results reported previously but contrary with results of NEYF doped CZTSSe [35–38]. Above results indicate that effect of NEYF doping on electrical properties of CZTSSe solar cell does not mainly come from Na-related passivation but may come from decreased V_{Cu} due to formation of more [V_{Cu} + Zn_{Cu}] defect complex. It is known from discussions about Fig. 3 and data shown in Table 2 that NEYF doping make CZTSSe further Cu poorer but Zn richer, which leads to more [V_{Cu} + Zn_{Cu}] defect complex formed. Since [V_{Cu} + Zn_{Cu}] defect complex is electrical neutral, formation of more [V_{Cu} + Zn_{Cu}] defect complex implies decrease in V_{Cu} acceptor content and decrease in hole concentration. However, this question still need further study.

The decreased carrier density will lead to broader depletion region of CZTSSe/CdS, improve segregation ability of hole-electron pair and thus increase J_L. Therefore, the increased J_L of the CZTSSe:NEYF solar cells is due to decreased hole density of CZTSSe induced by NEYF doping, compared to CZTSSe solar cells. Combined with data in Table S1, this could also explain that J_{SC} of the CZTSSe:Na solar cells

Table 3
The electrical parameters of the CZTSSe, CZTSSe@5 mg, CZTSSe@10 mg thin films measured by Hall effect.

Samples	CZTSSe	CZTSSe@5 mg	CZTSSe@10 mg
Resistivity (Ω·cm)	45.6	63.6	205
Carrier density (cm^{-3})	1.04×10^{18}	1.09×10^{17}	1.39×10^{16}
Mobility (cm^2/Vs)	0.54	2.24	2.36
Type	p	P	p

decreases with increasing Na doping content. From the statements above, it is deduced that the improvement of J_{SC} of CZTSSe:NEYF solar cells should be attributed to NEYF nanoparticles, other than the concomitant Na.

It is also found from Table 3 that the resistivity increases with increasing NEYF content. It is known that increase in resistivity of absorber should lead to increased R_s of corresponding solar cell device. However, compared to CZTSSe solar cells, CZTSSe:NEYF solar cells have lower R_s, which indicates that the influence of NEYF doping on devices' R_s comes from change in electric properties of CZTSSe/Mo interfaces. It is demonstrated in Fig. 3 that the thickness of $MoSe_2$ layer at CZTSSe/Mo interface is much larger than that at CZTSSe:NEYF/Mo, which implies that the R_s induced by $MoSe_2$ is larger in CZTSSe solar cells than in CZTSSe:NEYF solar cells. Therefore, it is deduced that the decreased R_s should not be attributed to resistivity change of CZTSSe but the decrease in thickness of the $MoSe_2$ layer.

It can be seen from Table 2 that atomic ratio of Na in NEYF of NEYF doped CZTSSe films is much less than that in pure NEYF. We deduced that the decreased Na diffuse to surface of the NEYF doped CZTSSe films. In order to identify this deduction and understand effect of CZTSSe/CdS interface on solar cell, XPS measurement was performed for CZTSSe@5 mg and CZTSSe thin films. Fig. S6, S7 and S8 (in Supporting Information) in the supporting information show XPS spectra of elements in CZTSSe@5 mg thin film and CZTSSe thin film, respectively, from which atomic ratios of each element in CZTSSe@5 mg and CZTSSe thin films are extracted, as listed in Table 4. It is noted that no Er signal is detected the surface of the CZTSSe@5 mg thin film, implying that Er content is too little to be found at the surface. The atomic percent ratios of F, Na and Y among the three elements are 28.3, 40.8 and 30.9 at%, respectively. The ratio of Na is much larger than that of pure NEYF (20.87 at%) and of the NEYF in the bulk of CZTSSe@5 mg (8.1 at%) thin film. Based on previously reported literatures and statements above, it is deduced that the increased Na at the surface comes from Na diffused from the absorber and SLG substrate [39]. As illustrated in many previous reports, the Na could passivate the donor defects at interface, and reduce interfacial recombination [40–42]. The excessive Na can passivate defects on surface, leading to decrease in interface recombination rate J_0 compared to CZTSSe solar cells. The F ratio decreases from 52.6 at% of pure NEYF to 28.1 at%. While the Y ratio increases from 19.35 at% of pure NEYF to 30.7 at%.

It can be seen that there are two types of Se at the surface of the CZTSSe:NEYF thin film, one type is attributed to CZTSSe, and another to elemental Se. The atomic ratios of Cu, Zn, Sn and Se for the CZTSSe thin film and CZTSSe in the CZTSSe@5 mg thin film are calculated, as listed in second column and fourth columns of Table 4, respectively. Obviously, the surface of the CZTSSe@5 mg thin film has lower Cu and Se content than the surface of the CZTSSe, which means that the surface of the CZTSSe@5 mg thin film deviates from stoichiometric ratio of formation of single-phase kesterite CZTSSe more seriously than the surface of the CZTSSe thin film. Therefore, it is indicated that the surface of the CZTSSe@5 mg thin film will have more defects and secondary phases than that of the CZTSSe thin film, which leads to the CZTSSe:NEYF solar cell has larger shunt conductivity than CZTSSe solar cell, in agreement with results in Table 1.

Table 4
Surface element ratio of CZTSSe thin film and CZTSSe@5 mg thin film measured by XPS.

Samples	CZTSSe@5 mg	CZTSSe of CZTSSe@5 mg	NEYF of CZTSSe@5 mg	CZTSSe
Cu at%	6.8	12.2	–	16
Zn at%	13.5	24.3	–	14
Sn at%	13.2	23.8	–	18
Se(CZTSSe) at%	22.1	39.7	–	52
Se(elemental) at%	13.1	–	–	–
F at%	8.8	–	28.1	–
Na at%	12.7	–	41	–
Y at%	9.6	–	30.7	–
Er at%	0	–	0	–

Notes: The data in CZTSSe of CZTSSe@5 mg column shows atomic percent of Cu, Zn, Sn, S and Se in CZTSSe@5 mg thin films without taking F, Na, Y and Er into account; The data in NEYF of CZTSSe@5 mg column shows atomic percent of F, Na, Y and Er in CZTSSe@5 mg thin films without taking Cu, Zn, Sn, S and Se into account.

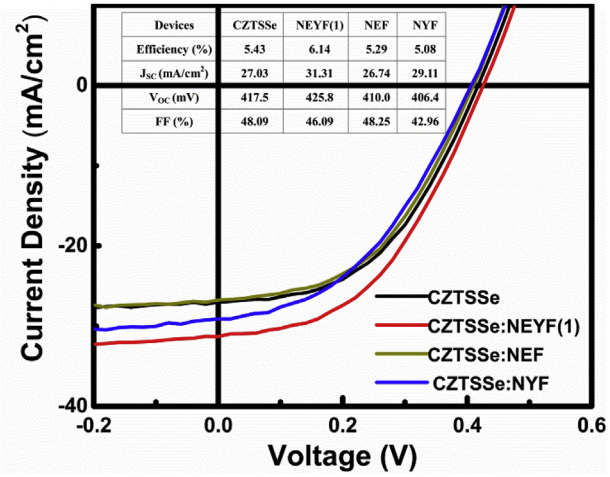

Fig. 4. J–V curves and Photovoltaic parameters of CZTSSe (black), CZTSSe:NEYF(1) (red), CZTSSe:NEF (grey) and CZTSSe:NYF (blue) solar cells. (For interpretation of the references to colour in this figure legend, the reader is referred to the Web version of this article.)

The core-shell NEYF consists of $NaErF_4$ (NEF) core with diameter in 20 nm and $NaYF_4$ (NYF) shell with thickness in 5 nm. It is evitable that NEF and NYF impose their influences on CZTSSe solar cells when doped as a part of core-shell NEYF. For further understanding effect from the core-shell structure of NEYF on performance of CZTSSe based solar cell, four CZTSSe based solar cells were prepared with NEF-, NYF and NEYF doped CZTSSe as absorbers, respectively, and denoted as CZTSSe:NEF, CZTSSe:NYF and CZTSSe:NEYF(1), respectively. Fig. 4 reveals J-V curves of CZTSSe, CZTSSe:NEF, CZTSSe:NYF and CZTSSe:NEYF(1) solar cells, from which the photovoltaic parameters of the three solar cells are extracted, as listed in Fig. 4.

It is found that CZTSSe:NEYF(1) solar cell has better J_{SC}, V_{OC} and PCE than CZTSSe solar cell, in agreement with result of Fig. 1(a). In contrast, the CZTSSe:NEF solar cell has lower J_{SC}, V_{OC} and PCE than the CZTSSe solar cell, indicating that NEF doping cannot improve performance of CZTSSe solar cell. For the CZTSSe:NYF solar cell, even sharing common NYF dissolving effect and enhanced Jsc with CZTSSe:NEYF solar cell, it doesn't possess better performance than CZTSSe solar cell. These results indicate that individual NEF and NYF doping cannot increase PCE of CZTSSe solar cell, while increase in the PCE induced by NEYF doping may come from NYF dissolution and action of core-shell NEYF. However, corresponding mechanism still need further investigation.

4. Conclusions

Three kinds of CZTSSe, CZTSSe:NEYF and CZTSSe/NEYF solar cells were prepared. It is found that NEYF doping can increase V_{OC}, J_{SC} and FF of the CZTSSe:NEYF solar cell, which enables the PCE increase from 4.03% of CZTSSe solar cell up to 7.10%, while NEYF inserting improves the PCE of CZTSSe/NEYF solar cell little. The increased V_{OC} is due to decreased J_0 and increased J_L, the increased J_{SC} to decrease in E_g and J_0 and increased J_L, and the increased FF to decrease in R_s. Compared to CZTSSe solar cells, the decreased E_g of CZTSSe:NEYF solar cells should be ascribed to the decreased S/(S + Se) ratio; the decreased J_0 to

passivation of superficial defects by Na coming from NEYF; the decreased R_s to that its $MoSe_2$ layer thickness is much less than that of CZTSSe solar cell; and increased J_L to decrease in hole density induced by NEYF doping.

Acknowledgement

This work is supported by the National Natural Science Foundation of China under Grant Nos. 61774075; The Science and Technology Development Project of Jilin Province under grant No. 20170101142JC, Natural Science Foundation of Jilin Province under grant No. 20180101227JC. This work was also supported by High Performance Computing Center of Jilin University, China.

Appendix A. Supplementary data

Supplementary data to this article can be found online at https://doi.org/10.1016/j.solmat.2019.110175.

References

[1] M.A. Green, Y. Hishikawa, E.D. Dunlop, D.H. Levi, J. Hohl-Ebinger, M. Yoshita, A.W.Y. Ho-Baillie, Solar cell efficiency tables (Version 53), Prog. Photovolt. Res. Appl. 27 (2019) 3–12.
[2] W. Wang, M.T. Winkler, O. Gunawan, T. Gokmen, T.K. Todorov, Y. Zhu, D.B. Mitzi, Device characteristics of CZTSSe thin-film solar cells with 12.6% efficiency, Adv. Energy Mater. 4 (2014).
[3] D.B. Mitzi, O. Gunawan, T.K. Todorov, D.A. Barkhouse, Prospects and performance limitations for Cu-Zn-Sn-S-Se photovoltaic technology, Philos. Trans. Ser. A Math. Phys. Eng. Sci. 371 (2013) 20110432.
[4] T. Gokmen, O. Gunawan, T.K. Todorov, D.B. Mitzi, Band tailing and efficiency limitation in kesterite solar cells, Appl. Phys. Lett. 103 (2013) 103506.
[5] S. Bourdais, C. Choné, B. Delatouche, A. Jacob, G. Larramona, C. Moisan, A. Lafond, F. Donatini, G. Rey, S. Siebentritt, A. Walsh, G. Dennler, Is the Cu/Zn disorder the main culprit for the voltage deficit in kesterite solar cells? Adv. Energy Mater. 6 (2016) 1502276.
[6] G. Altamura, J. Vidal, Impact of minor phases on the performances of CZTSSe thin-film solar cells, Chem. Mater. 28 (2016) 3540–3563.
[7] Z. Tong, K. Zhang, K. Sun, C. Yan, F. Liu, L. Jiang, Y. Lai, X. Hao, J. Li, Modification of absorber quality and Mo-back contact by a thin Bi intermediate layer for kesterite Cu_2ZnSnS_4 solar cells, Sol. Energy Mater. Sol. Cells 144 (2016) 537–543.
[8] S. López-Marino, M. Placidi, A. Pérez-Tomás, J. Llobet, V. Izquierdo-Roca, X. Fontané, A. Fairbrother, M. Espíndola-Rodríguez, D. Sylla, A. Pérez-Rodríguez, E. Saucedo, Inhibiting the absorber/Mo-back contact decomposition reaction in $Cu_2ZnSnSe_4$ solar cells: the role of a ZnO intermediate nanolayer, J. Mater. Chem. 1 (2013).
[9] A. Cabas-Vidani, S.G. Haass, C. Andres, R. Caballero, R. Figi, C. Schreiner, J.A. Márquez, C. Hages, T. Unold, D. Bleiner, A.N. Tiwari, Y.E. Romanyuk, High-efficiency $(Li_xCu_{1-x})_2ZnSn(S,Se)_4$ kesterite solar cells with lithium alloying, Adv. Energy Mater. 8 (2018).
[10] H. Xie, S. Lopez-Marino, T. Olar, Y. Sanchez, M. Neuschitzer, F. Oliva, S. Giraldo, V. Izquierdo-Roca, I. Lauermann, A. Perez-Rodriguez, E. Saucedo, Impact of Na dynamics at the $Cu_2ZnSn(S,Se)_4$/CdS interface during post low temperature treatment of absorbers, ACS Appl. Mater. Interfaces 8 (2016) 5017–5024.
[11] Y. Wu, M. Zhao, D. Zhuang, N. Zhang, X. Yu, Y. Wei, X. Lyu, G. Ren, C. Wang, L. Hu, Y. Li, J. Wei, Q. Gong, The effect of Rb doping on CZTSSe solar cells, Sol. Energy 187 (2019) 269–273.
[12] Y.-F. Qi, D.-X. Kou, W.-H. Zhou, Z.-J. Zhou, Q.-W. Tian, Y.-N. Meng, X.-S. Liu, Z.-L. Du, S.-X. Wu, Engineering of interface band bending and defects elimination via a Ag-graded active layer for efficient $(Cu,Ag)_2ZnSn(S,Se)_4$ solar cells, Energy Environ. Sci. 10 (2017) 2401–2410.
[13] X. Chen, W. Xu, H. Song, C. Chen, H. Xia, Y. Zhu, D. Zhou, S. Cui, Q. Dai, J. Zhang, Highly efficient LiYF4:Yb^{3+},Er^{3+} upconversion single crystal under solar cell spectrum excitation and photovoltaic application, ACS Appl. Mater. Interfaces 8 (2016) 9071–9079.
[14] S. Fischer, E. Favilla, M. Tonelli, J.C. Goldschmidt, Record efficient upconverter solar cell devices with optimized bifacial silicon solar cells and monocrystalline BaY_2F_8: 30%Er^{3+} upconverter, Sol. Energy Mater. Sol. Cells 136 (2015) 127–134.
[15] J. Yu, Y. Yang, R. Fan, D. Liu, L. Wei, S. Chen, L. Li, B. Yang, W. Cao, Enhanced near-infrared to visible upconversion nanoparticles of Ho^{3+}-Yb^{3+}-F^- tri-doped TiO (2) and its application in dye-sensitized solar cells with 37% improvement in power conversion efficiency, Inorg. Chem. 53 (2014) 8045–8053.
[16] J. Zuo, Q. Li, B. Xue, C. Li, Y. Chang, Y. Zhang, X. Liu, L. Tu, H. Zhang, X. Kong, Employing shells to eliminate concentration quenching in photonic upconversion nanostructure, Nanoscale 9 (2017) 7941–7946.
[17] H. Zhou, T.B. Song, W.C. Hsu, S. Luo, S. Ye, H.S. Duan, C.J. Hsu, W. Yang, Y. Yang, Rational defect passivation of $Cu_2ZnSn(S,Se)_4$ photovoltaics with solution-processed Cu_2ZnSnS_4:Na nanocrystals, J. Am. Chem. Soc. 135 (2013) 15998–16001.
[18] X. Zhang, D. Han, S. Chen, C. Duan, J. Chu, First-principles study on the alkali chalcogenide secondary compounds in $Cu(In,Ga)Se_2$ and $Cu2ZnSn(S,Se)_4$ thin film solar cells, J. Energy Chem. 27 (2018) 1140–1150.
[19] P. Jackson, R. Wuerz, D. Hariskos, E. Lotter, W. Witte, M. Powalla, Effects of heavy alkali elements in $Cu(In,Ga)Se_2$ solar cells with efficiencies up to 22.6%, Phys. Status Solidi Rapid Res. Lett. 10 (2016) 583–586.
[20] H.-S. Qian, Y. Zhang, Synthesis of hexagonal-phase Core − Shell $NaYF_4$ nanocrystals with tunable upconversion fluorescence, Langmuir 24 (2008) 12123–12125.
[21] N. Aihara, H. Araki, A. Takeuchi, K. Jimbo, H. Katagiri, Fabrication of Cu_2SnS_3 thin films by sulfurization of evaporated Cu-Sn precursors for solar cells, Phys. Status Solidi 10 (2013) 1086–1092.
[22] J.F. Suyver, J. Grimm, M.K. van Veen, D. Biner, K.W. Krämer, H.U. Güdel, Upconversion spectroscopy and properties of $NaYF_4$ doped with Er^{3+}, Tm^{3+} and/or Yb^{3+}, J. Lumin. 117 (2006) 1–12.
[23] R. Shannon, Revised effective ionic radii and systematic studies of interatomic distances in halides and chalcogenides, Acta Crystallogr. A 32 (1976) 751–767.
[24] T. Gershon, B. Shin, N. Bojarczuk, M. Hopstaken, D.B. Mitzi, S. Guha, The role of sodium as a surfactant and suppressor of non-radiative recombination at internal surfaces in Cu_2ZnSnS_4, Adv. Energy Mater. 5 (2015).
[25] Y. Yang, L. Huang, D. Pan, New insight of Li-doped $Cu_2ZnSn(S,Se)_4$ thin films: Li-induced Na diffusion from soda lime glass by a cation-exchange reaction, ACS Appl. Mater. Interfaces 9 (2017) 23878–23883.
[26] S. Chen, L.-W. Wang, A. Walsh, X.G. Gong, S.-H. Wei, Abundance of Cu_{Zn} + Sn_{Zn} and $2Cu_{Zn}$ + Sn_{Zn} defect clusters in kesterite solar cells, Appl. Phys. Lett. 101 (2012).
[27] G. Altamura, M. Wang, K.L. Choy, Influence of alkali metals (Na, Li, Rb) on the performance of electrostatic spray-assisted vapor deposited $Cu_2ZnSn(S,Se)_4$ solar cells, Sci. Rep. 6 (2016) 22109.
[28] J. He, L. Sun, S. Chen, Y. Chen, P. Yang, J. Chu, Composition dependence of structure and optical properties of $Cu_2ZnSn(S,Se)_4$ solid solutions: an experimental study, J. Alloy. Comp. 511 (2012) 129–132.
[29] S. Levcenco, D. Dumcenco, Y.P. Wang, Y.S. Huang, C.H. Ho, E. Arushanov, V. Tezlevan, K.K. Tiong, Influence of anionic substitution on the electrolyte electroreflectance study of band edge transitions in single crystal $Cu_2ZnSn(S_xSe_{1-x})_4$ solid solutions, Opt. Mater. 34 (2012) 1362–1365.
[30] S. Chen, A. Walsh, J.-H. Yang, X.G. Gong, L. Sun, P.-X. Yang, J.-H. Chu, S.-H. Wei, Compositional dependence of structural and electronic properties of $Cu_2ZnSn(S,Se)_4$ alloys for thin film solar cells, Phys. Rev. B 83 (2011) 125201.
[31] M. Dimitrievska, A. Fairbrother, E. Saucedo, A. Pérez-Rodríguez, V. Izquierdo-Roca, Influence of compositionally induced defects on the vibrational properties of device grade $Cu_2ZnSnSe_4$ absorbers for kesterite based solar cells, Appl. Phys. Lett. 106 (2015).
[32] J. Li, S. Kim, D. Nam, X. Liu, J. Kim, H. Cheong, W. Liu, H. Li, Y. Sun, Y. Zhang, Tailoring the defects and carrier density for beyond 10% efficient CZTSe thin film solar cells, Sol. Energy Mater. Sol. Cells 159 (2017) 447–455.
[33] J. Márquez, M. Neuschitzer, M. Dimitrievska, R. Gunder, S. Haass, M. Werner, Y.E. Romanyuk, S. Schorr, N.M. Pearsall, I. Forbes, Systematic compositional changes and their influence on lattice and optoelectronic properties of $Cu_2ZnSnSe_4$ kesterite solar cells, Sol. Energy Mater. Sol. Cells 144 (2016) 579–585.
[34] M. Dimitrievska, S. Giraldo, P. Pistor, E. Saucedo, A. Pérez-Rodríguez, V. Izquierdo-Roca, Raman scattering analysis of the surface chemistry of kesterites: impact of post-deposition annealing and Cu/Zn reordering on solar cell performance, Sol. Energy Mater. Sol. Cells 157 (2016) 462–467.
[35] Y.-T. Hsieh, Q. Han, C. Jiang, T.-B. Song, H. Chen, L. Meng, H. Zhou, Y. Yang, Efficiency enhancement of $Cu_2ZnSn(S,Se)_4$ solar cells via alkali metals doping, Adv. Energy Mater. 6 (2016).
[36] Y. Li, Q. Han, T.W. Kim, W. Shi, The optical influence of Na on $Cu_2ZnSnSe_4$ films deposited with Na-containing sol–gel precursor, J. Sol. Gel Sci. Technol. 69 (2013) 260–265.
[37] A. Nagaoka, H. Miyake, T. Taniyama, K. Kakimoto, Y. Nose, M.A. Scarpulla, K. Yoshino, Effects of sodium on electrical properties in Cu_2ZnSnS_4 single crystal, Appl. Phys. Lett. 104 (2014).
[38] A. Nagaoka, M.A. Scarpulla, K. Yoshino, Na-doped Cu_2ZnSnS_4 single crystal grown by traveling-heater method, J. Cryst. Growth 453 (2016) 119–123.
[39] Y.-R. Lin, V. Tunuguntla, S.-Y. Wei, W.-C. Chen, D. Wong, C.-H. Lai, L.-K. Liu, L.-C. Chen, K.-H. Chen, Bifacial sodium-incorporated treatments: tailoring deep traps and enhancing carrier transport properties in Cu_2ZnSnS_4 solar cells, Nano Energy 16 (2015) 438–445.
[40] X. Zhang, D. Han, S. Chen, C. Duan, J. Chu, First-principles study on the alkali chalcogenide secondary compounds in $Cu(In,Ga)Se_2$ and $Cu2ZnSn(S,Se)_4$ thin film solar cells, J. Energy Chem. 27 (2018) 1140–1150.
[41] Y. Yang, X. Kang, L. Huang, S. Wei, D. Pan, A general water-based precursor solution approach to deposit earth abundant $Cu_2ZnSn(S,Se)_4$ thin film solar cells, J. Power Sources 313 (2016) 15–20.
[42] S. López-Marino, Y. Sánchez, M. Espíndola-Rodríguez, X. Alcobé, H. Xie, M. Neuschitzer, I. Becerril, S. Giraldo, M. Dimitrievska, M. Placidi, L. Fourdrinier, V. Izquierdo-Roca, A. Pérez-Rodríguez, E. Saucedo, Alkali doping strategies for flexible and light-weight $Cu_2ZnSnSe_4$ solar cells, J. Mater. Chem. 4 (2016) 1895–1907.